PROGRESS IN PHOTOVOLTAICS: RESEARCH AND APPLICATIONS
Prog. Photovolt: Res. Appl. 2002; **10**:257–269 (DOI: 10.1002/pip.408)

Research

Analysis of Quantum Efficiency and Optical Enhancement in Amorphous Si p–i–n Solar Cells

Steven S. Hegedus[1,*,†] and Ruhi Kaplan[1,2]
[1]*Institute of Energy Conversion, University of Delaware, Newark, DE 19716, USA*
[2]*Permanent address: Department of Physics, University of Mersin, Ciftlikkoy Campus, Mersin, Turkey*

The effect of* i*-layer thickness, tin oxide texture, and back reflector (BR) on optical enhancement has been systematically studied in a series of 20 a-Si p–i–n solar cells. The internal quantum efficiency has been analyzed by a simple model based on the work of Schade and Smith. The enhancement of optical absorption is characterized by* m*, a wavelength-dependent fitting parameter representing the increase in optical pathlength relative to the* i*-layer thickness* d*. Solar cells with an Al BR have negligible optical enhancement, with* $\mathbf{m} < 1{\cdot}5$*, consistent with large parasitic absorption at the Al/Si interface as reported by others. Solar cells on highly textured SnO_2 with ZnO/Al or ZnO/Ag BR have peak values of* $\mathbf{m} \sim 3$–4*, with ZnO/Ag having slightly larger values than ZnO/Al. It was found that* m *has a strong dependence on the product* αd*, and that maximum values of* m *increase with reflectivity of the BR. It is shown that a major source of parasitic absorption loss at long wavelengths is light trapping in the textured SnO_2 front contact. Copyright* © *2002 John Wiley & Sons, Ltd.

1. INTRODUCTION

Optical enhancement in a-Si solar cells is a well-known technique to increase the absorption efficiency of weakly absorbed light, and is critical for improving the performance of single or multijunction *p–i–n* or *n–i–p* devices. Effective optical enhancement of a-Si devices allows the use of a thinner *i*-layer to achieve the same photocurrent J_{PH} as a thicker solar cell, but with the advantage of better stability and faster manufacturing throughput. Optical enhancement increases the optical pathlength so that the device has an effective optical thickness of ($\boldsymbol{m}\ d$) where d is the physical thickness of the *i*-layer. The parameter $\boldsymbol{m}$ represents the increase in absorption length, and is a measure of the optical enhancement for weakly absorbed light due to both oblique scattering and multiple passes. The theoretical thermodynamic upper limit[1] is $\boldsymbol{m} \sim 4n^2$ where n is the index of refraction of the absorber. With $n \sim 4$ for a-Si, the upper limit for $\boldsymbol{m}$ is ~ 60 but this decreases rapidly to $\sim$10–20 with even a few per cent losses due to parasitic absorption at the interfaces.[1]

* Correspondence to: Steven S. Hegedus, Institute of Energy Conversion, University of Delaware, Newark, DE 19716, USA.
†E-mail: ssh@udel.edu

Contract/grant sponsor: NREL; contract/grant number: ZAK-8-17619-33.
Contact/grant sponsor: Fulbright Scholar Program.

Published online 28 January 2002

Received 20 February 2001
Revised 13 September 2001

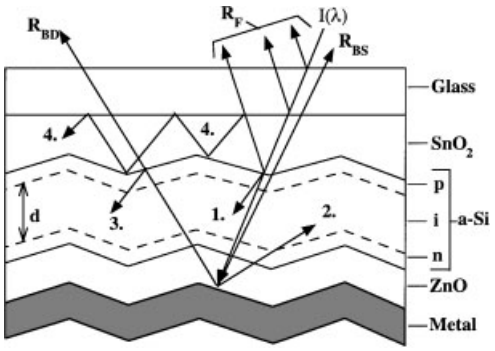

Figure 1. Diagram showing light trapping in *p–i–n* structure. Incident light $I(\lambda)$ can be reflected from the front interfaces R_F or absorbed in the *i*-layer before (ray 1) or after (rays 2 and 3) reflection at the back contact. Light which is reflected from the back, but which is not absorbed escapes via specular R_{BS} or diffuse R_{BD} reflection. The figure shows the light being reflected from the metal contact, whereas some is reflected from the Si/ZnO interface

There are two methods to increase the optical enhancement, or light trapping, and both must be achieved simultaneously to gain the full benefit. First, the substrate must be textured, which increases the pathlength by scattering the normally incident light at an angle away from normal, shown as ray 1 in Figure 1. Second, the back surface must be textured and have high reflectivity so that a large fraction of photons reaching that back contact are reflected and scattered back into the *i*-layer without losses (rays 2 and 3 of Figure 1).

Studies of optical enhancement and light trapping in a-Si solar cells typically fall into one of two categories; 1. use of changes in the short-circuit current J_{SC} or the long-wavelength quantum efficiency (QE) as an empirical measure of the optical enhancement;[3–8] or 2. Use of an optical model based on detailed calculations of the reflection, absorption, transmission, and scattering at each interface, using either coherent wave theory or geometric ray optics treatment to characterize the optical behavior of the multilayer structure.[9–14] This paper bridges the gap between the empirical and the theoretical approaches by presenting a quantitative analysis of the QE of a wide range of a-Si *p–i–n* solar cell device structures. The measured QE data at long wavelengths is fit with a simple, analytical model having one adjusted parameter $\boldsymbol{m}$ as a function of wavelength. All other optical characteristics of the device are measured separately and incorporated in the analysis. The experimental variables investigated include the *i*-layer thickness *d* from 0·14 to 0·92 μm, the SnO_2 texture (lightly textured or very textured), and the back reflector (BR) structure (Al, ZnO/Al, or ZnO/Ag). We analyze the optically limited internal QE, obtained at sufficiently large reverse bias that we can neglect recombination losses. Although these results were obtained from single-junction a-Si solar cells, they are also applicable to a multi-junction configuration where the light trapping occurs in the a-SiGe bottom cell.

2. EXPERIMENTAL

2a. Device fabrication

Single-junction *p–i–n* solar cells were deposited by r.f. plasma CVD. The device structure was glass/SnO_2/*p–i–n*/BR. The *p*-layers were ∼15-nm-thick a-SiC:H, followed by an undoped a-SiC buffer layer of similar thickness, and the *n*-layer was 20-nm-thick μc-Si. Five *p–i–n* device depositions were made with identical conditions, except for the *i*-layer time, giving devices with $d = 0{\cdot}14$, 0·28, 0·39, 0·62 and 0·92 μm. In each run there were three were Asahi-type-U highly textured SnO_2 and one lightly textured SnO_2, which will be referred to respectively as HTX (highly textured) and LTX (lightly textured). The HTX was 0·8 and the LTX was 0·4 μm thick. We have previously reported structural, optical and electronic characterization of these two SnO_2 materials.[15] Depositions of the individual *p*, *i*, and *n*-layers were also made on 7059 glass to characterize their optical absorption.

The devices were completed by depositing one of three different BR contacts. From each a-Si device run, one sample on HTX SnO_2 and one sample on LTX SnO_2 received evaporated Al contacts, while samples on the other two HTX substrates received ZnO/Al and ZnO/Ag contacts. The ZnO was 80 nm thick and was sputtered in Ar/O_2 at 3 mT from an Al-doped target. The Al and Ag were e-beam evaporated. The cell areas were 0·4 cm^2. Details of the deposition and electrical and optical properties of these types of BR's are given elsewhere.[16]

2b. Optical absorption and reflection measurements

Transmission T and reflection R were measured on Si p, i, and n films, deposited on glass, using a spectrophotometer with an integrating sphere. Absorption of the smooth and textured SnO_2 was obtained from the measurements of the transmission and reflection, using the liquid index matching method.[15]

Values of α for the various Si layers were obtained from the measured T and R by an iterative approach.[17] A very good fit to the absorption data was obtained[18] with the expression:

$$(\alpha E)^{0.33} = B(E - E_0) \tag{1}$$

with $B = 77\ \mathrm{cm}^{-1/3}\mathrm{eV}^{-2/3}$ and $E_0 = 1{\cdot}53$ eV over the range 1·7–2·6 eV. When plotted as $(\alpha \mathrm{E})^{0.5}$, as in the more commonly used Tauc method, a Tauc bandgap of 1·71 eV resulted, but the fit was not as good.

Figures 2(a, b) shows the total, diffuse and specular reflection from the glass side of the completed p–i–n devices ($d = 0{\cdot}93$ μm) on HTX and LTX SnO_2, respectively. Also shown are the total reflection measured from

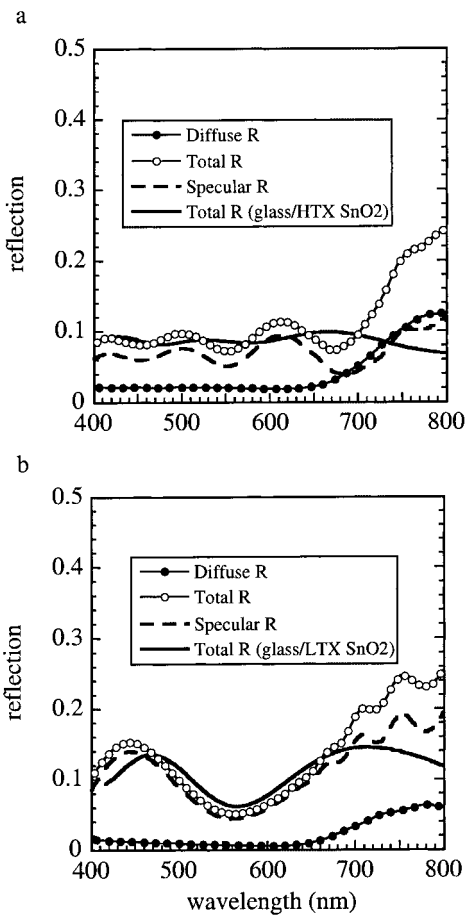

Figure 2. Total, diffuse and specular reflection from the glass side of glass/SnO_2/p–i–n/Al devices with $d = 0{\cdot}92$ μm on HTX (a) and LTX SnO_2 (b). Also shown is the total reflection from the glass side of glass/SnO_2

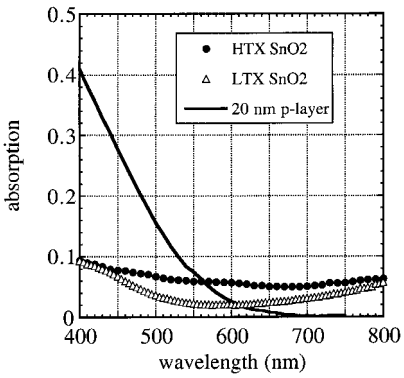

Figure 3. Absorption of HTX and LTX SnO_2 (obtained with index matching liquid) and the *p*-layer

the front glass surface of each type of textured SnO_2 , without a *p–i–n* device (R_F in Figure 1). The LTX SnO_2 (Figure 2b) has more pronounced fringing, as expected since there was more specular reflection. For each type of SnO_2, the total reflection from the glass/SnO_2 and the glass/SnO_2/*p–i–n*/Al structures are very similar up to about 650 nm, indicating that R_F for both is governed by reflection from the air/glass and glass/SnO_2 interfaces. Averaging the reflection fringes gives R_F values of 0·08 for the HTX and 0·10 for the LTX SnO_2. These averaged values will be used in Section 4. Beyond 650 nm, the measured *R* for the *p–i–n* device samples increases due to the light which is reflected at the BR, but not trapped. For the LTX sample (Figure 2b), this increase is due mostly to specular reflection. For the HTX sample (Figure 2a), this increase is due mostly to diffuse reflection.

The absorption of the SnO_2 was obtained using an index matching liquid to eliminate multiple internal reflections. We used an index matching liquid with $n = 1{\cdot}70$ and corrected for absorption in the liquid or cover slide.[15] Figure 3 shows the absorption for the LTX and HTX SnO_2/glass substrates. The LTX has approximately half the absorption in the range 500–700 nm because it is only half as thick as the HTX. This figure also shows the absorption in the *p*-layer.

The haze, defined as the ratio of diffuse to total transmission, is obtained from total and diffuse transmission measurements without index matching liquids. From 600 to 750 nm, the average haze for the HTX SnO_2 is 0·09 and for the LTX is 0·03.

2c. Solar cell electrical measurements

The illuminated current–voltage (*J–V*) performance was obtained under simulated AM1·5 global light from an Oriel solar simulator calibrated with a filtered (Schott KG5) c-Si cell. Table I shows the illuminated performance for the four pieces with different SnO_2 and BR from the same *p–i–n* deposition where $d = 0{\cdot}39\,\mu m$. Including results from all 20 devices in this study, the open-circuit voltages were 0·83–0·87 V, fill factors were 62–72%, and efficiencies were 6–9·3%, depending on thickness and contact.

Table I. Illuminated *J–V* results (AM1·5 global) for devices from deposition with $d = 0{\cdot}39\,\mu m$ for different BR on LTX or HTX SnO_2

SnO_2 haze	BR contact	V_{OC}(V)	J_{SC} (mA/cm^2)	Fill factor (%)	Efficiency (%)
LTX	Al	0·85	12·5	65·4	7·0
HTX	Al	0·85	13·1	69·8	7·7
HTX	ZnO/Al	0·86	14·1	72·0	8·7
HTX	ZnO/Ag	0·85	14·7	71·3	8·9

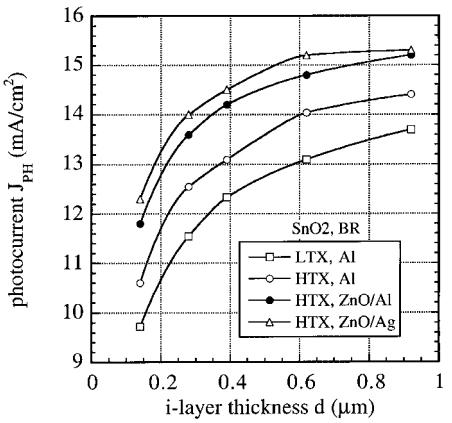

Figure 4. Dependence of photocurrent obtained from integration of measured QE(− V) with AM1·5 spectrum on thickness *d*, for all devices in this study

The QE system was calibrated with the same filtered c-Si device as was used to calibrate the simulator. The QE was measured with a reverse-bias voltage to establish a sufficiently high field in the *i*-layer so that the QE saturated. Thus, every photon absorbed in the *i*-layer generates a carrier, which is collected; i.e., electrical losses were negligible. The reverse bias necessary for saturation of the QE ranged from $-0{\cdot}2$ V for the devices with $d = 0{\cdot}14$ μm to -4 V for the devices with 0·92 μm. Figure 4 shows the dependence of J_{PH} on the *i*-layer thickness for all four device types. J_{PH}, which was obtained from integrating the QE at reverse bias with the AM1·5 spectrum, increases rapidly with *d* up to ~ 0.6 μm, then more gradually up to 0·92 μm. For the devices with the same Al BR, J_{PH} increases about 1 mA/cm^2 with the more textured HTX SnO_2 compared with LTX SnO_2. For the devices on the same HTX SnO_2, J_{PH} increases about another 1 mA/cm^2 for devices with the more reflective ZnO/Al BR compared with an Al BR.

Figure 5 shows the QE for the four devices having $d = 0{\cdot}39$ μm. The QE of the device with LTX SnO_2 has evidence of interference fringes, in contrast to the other three on HTX SnO_2. Interference results in the device with LTX having a lower QE between 400 and 500 nm due to reflection maximum, but a higher QE between 500 and 600 nm due to a reflection minimum, as shown in Figure 2(b). This is consistent with reports that a-Si solar cells on smooth substrates have a lower blue response due to increased front surface reflection losses.[6,8,19] The long-wavelength QE increases going from LTX to HTX, and from Al to ZnO/Al to ZnO/Ag BR. The three devices on HTX agree very well at short wavelengths since they have identical front surface reflection and absorption losses. This is confirmed by the agreement between the measured QE for all three and the

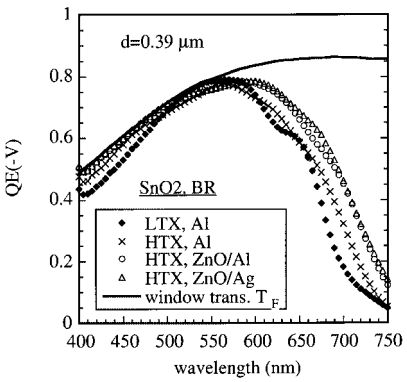

Figure 5. QE(− V) for devices with $d = 0{\cdot}39$ μm for all four combinations of device structures. The transmission into the *i*-layer T_F is also shown (see Equation 3)

transmission through the front layers into the *i*-layer, T_F, which will be discussed in the next section. In the following analysis, we will focus on the region from 600–750 nm where the optical enhancement occurs.

3. QUANTUM EFFICIENCY MODEL

The critical aspect in modeling the optically limited QE is to calculate the light absorbed in the *i*-layer due to light trapping (rays 2 and 3 in Figure 1). Following Schade & Smith,[9] the QE is:

$$QE = (1 - R_F)(1 - A_{TCO})(1 - A_p)(A_i)[1 + f(R_B)] \quad (2)$$

where A_{TCO}, A_P, and A_i are the absorbance of the TCO, *p*-layer, and *i*-layer, respectively, and $f(R_B)$ is the enhancement due to the back reflection, with R_B as the reflection coefficient for the BR contact.

Referring to Figure 1, a fraction of the incident light $I(\lambda)$ is reflected from the air/glass, glass/SnO_2 , and SnO_2/p interfaces before having a chance to be absorbed in the *p*-layer or *i*-layer. These three components of front surface reflection are grouped together as R_F. Figure 2(a, b) showed the total reflection from the devices on both types of SnO_2. The value of R_F at long wavelengths in Equation (2) is simply to account for the reflection losses at the front of the device, not the additional light reflected from the back which escapes as R_{BS} and R_{BD} of Figure 1.

Light is also absorbed in the SnO_2 (A_{TCO}) and in the *p*-layer (A_p). Figure 3 shows that the absorption loss in the *p*-layer dominates the QE at short wavelengths and is negligible beyond 600 nm, where the analysis of the optical enhancement is focused. The absorption in SnO_2 is relatively flat, and only a few per cent between 600–750 nm for a single pass of normal incidence light. However, light which is critically trapped in the SnO_2 can result in much greater percentage losses.

Thus, the fraction of incident light reaching the *i*-layer is given by the product of the transmission through each of the front 'window' layers, or:

$$T_F = (1 - R_F)(1 - A_{TCO})(1 - A_p) \quad (3)$$

Figure 5 shows that QE $\cong T_F$ up to where the QE begins to decrease due to fall-off at $\sim$550 nm caused by *i*-layer absorption. Equation (3) allows us to rewrite Equation (2) as

$$QE = (T_F)(A_i)[1 + f(R_B)] \quad (4)$$

which clearly shows the three main contributions to the QE, namely the transmission through the front layers, the absorption in the *i*-layer, and the back reflection.

Light entering the *i*-layer can be absorbed during its first pass, indicated by ray 1 in Figure 1. Light reaching the BR is either absorbed at that contact[10,13,20] or scattered back into the *i*-layer. Some of that light will be absorbed in the *i*-layer, as shown by ray 2 in Figure 1. Reflected light from a textured substrate is often scattered at an oblique angle. This increases its probability for absorption in the next pass, and for subsequent reflection at the SnO_2/p interface back into the *i*-layer. This increase in absorption for multiply scattered light in subsequent passes as shown by ray 3 in Figure 1, and represents very effective light trapping with $\boldsymbol{m} > 2$. If the weakly absorbed light was not scattered at either interface, the maximum would be $\boldsymbol{m} \sim 2$ since it would have at most two transits through the *i*-layer before escaping the front as specular back-reflected light R_{BS}, but with oblique scattering, $\boldsymbol{m}$ can exceed 2. Since $\boldsymbol{m}$ depends on scattering, absorption and reflection, which are all wavelength dependent, $\boldsymbol{m}$ must be wavelength dependent as well. Thus, the absorption in the *i*-layer is given by:

$$A_i = 1 - \exp(-\alpha \boldsymbol{m} d) \quad (5)$$

Rearrangement of the expression of Schade & Smith[9] gives the contribution of the back contact to the enhancement as:

$$f(R_B) = R_B(1 - A_i) = R_B \exp(-\alpha \boldsymbol{m} d) \quad (6)$$

Absorption in the *n*-layer is neglected here, consistent with other work.[9] This is well justified since it is ~ 7 times thinner than even the thinnest *i*-layer, and has negligible absorption[10] at 600–750 nm.

An alternative approach is discussed in the Appendix, where the effect of R_B is not represented explicitly, as in Equation (6), but is combined with $\boldsymbol{m}$ into a single parameter, representing the total enhancement.

R_B has been shown to be nearly independent of wavelength[9,20,21] in the range 600–750 nm for typical back reflectors used in a-Si solar cell technology. We confirmed this with reflection measurements on TCO/metal test structures and by simulation with PVOPTICS.[13] To determine the sensitivity of the procedure to the value of R_B, we applied two different versions of the analysis to fit the QE, selecting a device with $d = 0{\cdot}39\ \mu$m on HTX with a ZnO/Ag BR as an example. One version used a fixed value of $R_B = 0{\cdot}87$ and fitted only $\boldsymbol{m}$, while the other allowed both R_B and $\boldsymbol{m}$ to be fitted. The value of 0·87 was obtained from published data[21] as well as our own measurements. It was found that the fitted value of R_B fluctuated by $\pm 5\%$ about the fixed value in the range 600–750 nm. Figure 6(a) shows that the model was able to fit the measured QE for both cases of R_B within 1% and Figure 6(b) shows that the enhancement $\boldsymbol{m}$ was essentially identical for both cases of R_B. Therefore, in the rest of this study we use a fixed value of R_B, with values of $R_B = 0{\cdot}7$ for Al, 0·82 for ZnO/Al, and 0·87 for ZnO/Ag. These values are consistent with measurements[13,20,21] and calculations[21] of others, as well as our own. They are lower than the reflection of an Al or ZnO/metal surface into air because the higher index of a-Si layer enhances parasitic absorption losses at the BR.[13,20,21] The decision to use fixed values of R_B allows our analysis to focus on the wavelength dependence of the single fitted parameter $\boldsymbol{m}$.

The modeling proceeds by using measured or calculated values of all parameters except $\boldsymbol{m}$, which was then adjusted at each wavelength to obtain the best agreement between the measured QE and Equation (4) in the range 600–750 nm. Analysis started with $\boldsymbol{m} = 1$ and increased in increments of 0·1 until agreement between the measured QE and Equation (4) was within 1% (relative) or as small as possible. Typically, the agreement was within 1% at all wavelengths.

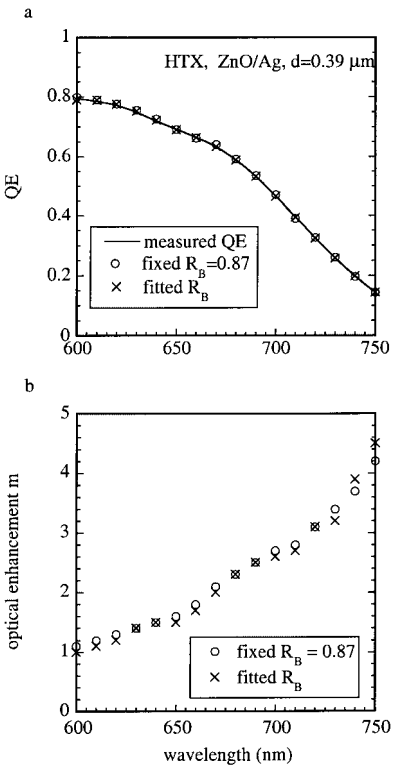

Figure 6. Results from analysis of one device ($d = 0{\cdot}39\ \mu$m on HTX SnO_2 with ZnO/Ag BR) for fixed plotted against value of R_B: (a) measured QE and calculated QE for fixed and fitted R_B; (b) enhancement $\boldsymbol{m}$ for the two cases from (a)

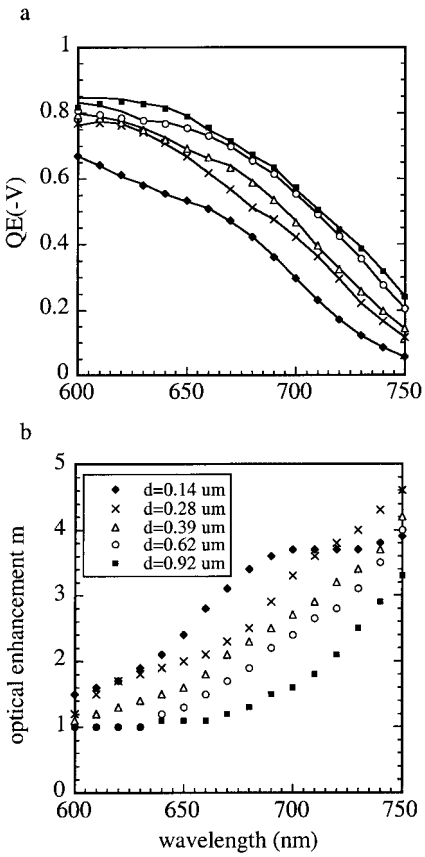

Figure 7. Results from analysis of five devices on HTX SnO_2 with ZnO/Ag BR, having $d = 0{\cdot}14$–$0{\cdot}92\,\mu m$; (a) measured (solid lines) and calculated (symbols) QE; (b) fitted values of enhancement $\boldsymbol{m}$

4. RESULTS

4a. Effect of i-layer thickness

Figure 7(a) shows the measured and fitted QE for a series of devices with $d = 0{\cdot}14$–$0{\cdot}92\,\mu m$. They were all deposited on HTX SnO_2 and had ZnO/Ag back reflectors. The fitted value of $\boldsymbol{m}$ for each device is shown in Figure 7(b). The wavelength where $\boldsymbol{m}$ begins to increase from unity increases with thickness d, indicating the point where light can be reflected from the back contact and trapped after multiple passes. This is expected to be approximately where $\alpha d \sim 1$ and will be discussed in Section 5. The value of $\boldsymbol{m}$ increases with wavelength, and saturates around 4 for the thinnest device, but continues to rise for the others.

4b. Effect of SnO_2 texture and back reflector

Figure 8(a, b) shows $\boldsymbol{m}$ for four devices having the thinnest and thickest *i*-layers studied here. The SnO_2 textured substrate and back reflector is different for each piece, as indicated in the figure. There is little optical enhancement with the Al BR for either the LTX or HTX SnO_2 for either the thinnest or thickest *i*-layer. Values of $\boldsymbol{m}$ are generally less than 1·5 with Al contacts on the LTX or HTX substrates for all device thicknesses studied here. This indicates a strong reduction in multiple passes due to the Al BR. For the thinner devices in Figure 8(a), $\boldsymbol{m}$ increases significantly with ZnO/metal contacts on HTX SnO_2 , saturating at $\boldsymbol{m} \sim 3$–4. For the thicker devices in Figure 8(b), $\boldsymbol{m}$ increases monotonically for the devices with ZnO/metal BR without saturating in the same range. Comparing ZnO/Al to ZnO/Ag in Figures 8(a, b), the ZnO/Ag BR enhances light trapping more in thin

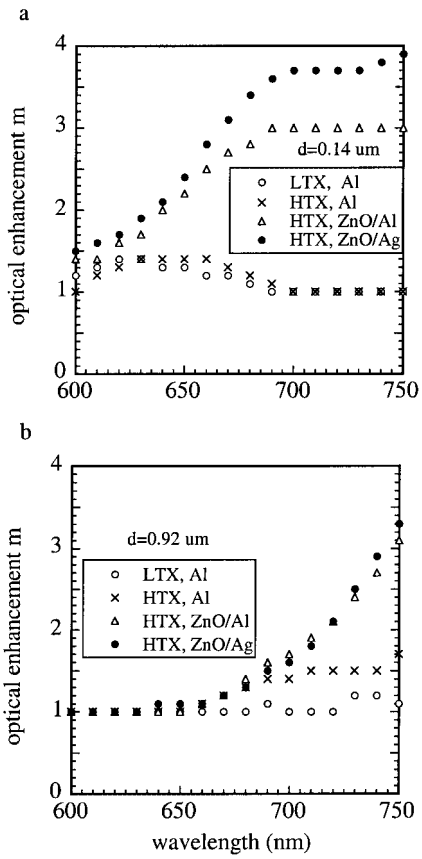

Figure 8. Enhancement $\boldsymbol{m}$ for devices with all four combination of SnO_2 and BR; (a) devices with $d = 0{\cdot}14\,\mu m$; (b) devices with $d = 0{\cdot}92\,\mu m$

devices than in thicker ones. Both figures indicate the critical importance of a ZnO (or any other TCO buffer layer) between the Si and metal layers for improving optical enhancement of the QE. Reasons for the beneficial effect of a dielectric layer between the metal contact and Si have been discussed.[13,16,20]

5. DISCUSSION

5a. Optical enhancement

Figures 7(b) and 8(a, b) show that for a given device structure, $\boldsymbol{m}$ decreases at a given wavelength with increasing thickness. This suggests that $\boldsymbol{m}$ depends on the product αd, not just on d. Figure 9(a–c) shows $\boldsymbol{m}$ as a function on αd at several wavelengths for the Al, ZnO/Al and ZnO/Ag BR on HTX substrates as d varies from 0·14 to 0·92 μm. Starting at high values of αd, i.e., short wavelengths, the figures clearly show that $\boldsymbol{m}$ begins to increase from 1 for αd just slightly greater than 1, as expected. With decreasing αd, $\boldsymbol{m}$ continues to increase, then saturates for very weakly absorbed light, $\alpha d < 0{\cdot}1$. The peak value of $\boldsymbol{m}$ increases with increasing reflectivity of the BR. These three figures clearly show the dependence of $\boldsymbol{m}$ on the back reflector, since they were deposited on the same HTX SnO_2.

The only previously published data showing the wavelength dependence of $\boldsymbol{m}$ found a very similar increase in $\boldsymbol{m}$, e.g., $\boldsymbol{m} \sim 3$ at 700 and $\boldsymbol{m} \sim 5$ at 750 nm, for a *p–i–n* device with ITO/Ag BR on highly textured SnO_2.[12] Other studies[9,22,23] estimate a wavelength-independent value of $\boldsymbol{m} \sim 3$–5. The good agreement between our results of $\boldsymbol{m} \sim 3$–4 and those from other groups suggests a fundamental loss common to all similarly fabricated

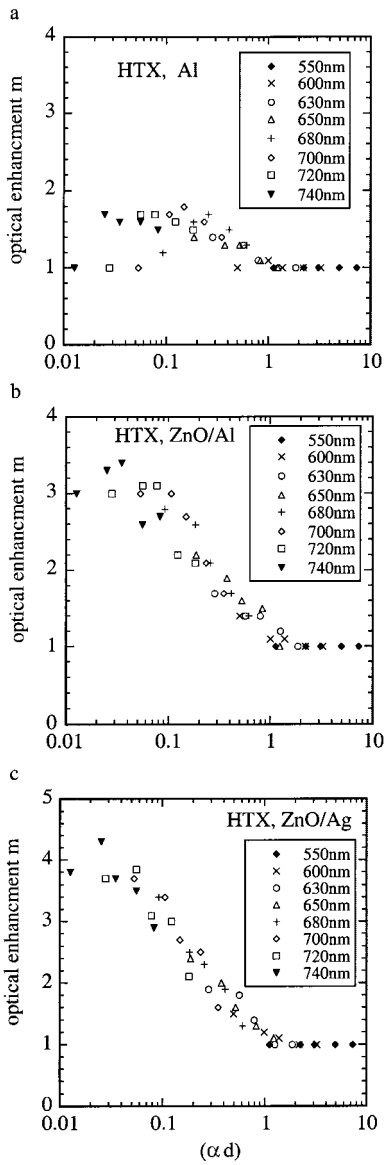

Figure 9. Enhancement ***m*** as a function of αd for devices on HTX SnO_2 at all thicknesses at selected wavelengths; (a) Al BR; (b) ZnO/Al BR; (c) ZnO/Ag BR

superstrate-type devices. Compared to theoretical values of $\boldsymbol{m} \sim 15$–20 expected for 10–20% parasitic absorption at the contacts,[1] these values of $\boldsymbol{m} \sim 3$–5 imply very large parasitic absorption losses for the *p–i–n* device structure.

5b. Optical losses

The effect of the back contact on parasitic absorption is clearly seen in Figure 10 which shows the total absorption for samples with the three different BRs used in this study along with bare a-Si (no BR). There are three different substrates represented; smooth glass, LTX SnO_2, and HTX SnO_2. Each has 0·5 μm a-Si layer. The structure was glass/(LTX or HTXSnO_2)/0·5 μm a-Si *i*-layer/BR or air. Some samples had no BR other than

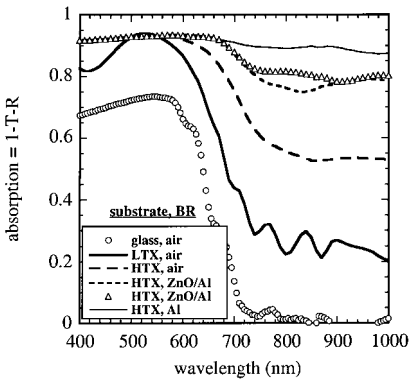

Figure 10. Absorption ($A = 1 - T - R$) in glass/HTX/a-Si/BR, glass/LTX/a-Si (solid line) or glass/a-Si (open circles) structures. The a-Si was 0·5 μm. Devices without BR contact listed as having 'air' as BR

air. Comparing first the samples with air as the BR (no contact) beyond 800 nm, absorption in the *i*-layer on smooth glass is $< 1\%$, absorption of the sample on LTX SnO_2 is about 25%, while HTX SnO_2 is greater than 50%. This indicates that the textured SnO_2 is responsible for a very significant fraction of the parasitical absorption. The absorption of the samples with a BR is greater than 70%. Figure 10 shows large parasitic absorption losses at the textured Al/Si interface[13] and that ZnO/Al reduces the absorption compared with Al, confirming the importance of a dielectric buffer between Si and metal.[4,13,17,21] There is only a slight difference between ZnO/Ag and ZnO/Al, as expected. However, even with no BR, absorption of about 50% of the light is unaccounted for beyond 800 nm with the HTX SnO_2.

Where is this light being absorbed? The most likely parasitic loss at long wavelengths is light absorbed in the textured SnO_2. Critical angle trapping inside the SnO_2 will lead to multiple internal reflections or light piping in the SnO_2. The weakly absorbed light will 'bounce around' until it is either reflected out of the glass, absorbed in the SnO_2, or absorbed at the back contact. The LTX SnO_2 had less of this effect, consistent with having less texture, hence light trapping. This suggests that in a solar cell, light which is reflected from the BR, but not absorbed in the *i*-layer, can be trapped in the SnO_2 (ray 4 in Figure 1), remaining there instead of reentering the *i*-layer (ray 3). These observations agree with Hishikawa *et al.*[23] who concluded that optical losses at long wavelengths were due to parasitic absorption in the textured SnO_2 which increased with optical confinement. Significant improvements in optical enhancement $\boldsymbol{m}$ and therefore J_{SC} will require a textured TCO with lower absorption than present-day SnO_2 and careful attention to the angle of the textured TCO sidewalls.

6. CONCLUSIONS

We have applied a simple model to analyze the measured QE of 20 a-Si *p–i–n* solar cells with a wide range of thickness, on low- and high-haze SnO_2 substrates, with three types of BR. The single fitting parameter $\boldsymbol{m}$ quantifies the optical enhancement by representing the additional path length for light at each wavelength before it is absorbed in the *i*-layer. For a given BR, $\boldsymbol{m}$ was inversely correlated with αd. Peak values of $\boldsymbol{m} \sim 1{\cdot}5$, 3 and 4 were found for BR of Al, ZnO/Al or ZnO/Ag, respectively. These are consistent with a few reports of other *p–i–n* cells, and are a factor of 4–6 times lower than predicted values, allowing for realistic absorption at contacts. Thus, present-day *p–i–n* a-Si solar cells have relatively poor light trapping. On the basis of the measured reflection of various BR structures, we conclude that parasitic absorption in the front textured TCO is responsible for the poor light trapping within the *i*-layer, not insufficient scattering or absorption at the back contact. Higher photocurrents will require lower textured TCO absorption as well as the increased reflectivity of the BR. Although all these results were obtained from single-junction a-Si solar cells, they are applicable to a multijunction configuration where the light trapping occurs in the a-SiGe bottom cell.

Acknowledgements

We thank W. Buchanan for the a-Si device deposition, K. Hart for ZnO and metal depositions, D. Eichenwald for programming the fitting algorithm in Excel, R. Birkmire for helpful comments, and H. Schade for careful reading, useful suggestions, and giving insight into the complexity of simplifying optical enhancement. This work was partially supported under NREL Subcontract ZAK-8-17619-33. One of the authors (RK) wishes to thank the Fulbright Scholar Program for support while at the Institute of Energy Conversion.

APPENDIX

Equations (5) and (6) separately model the effects of increased pathlength $\boldsymbol{m}$ and back reflection R_B, which together create the optical enhancement. However, these effects can be represented more simply by a single parameter $\boldsymbol{M}$ which includes the effect of all optical enhancement and can be related to the number of passes in the *i*-layer.[24] $\boldsymbol{M}$ can be related to the parameters $\boldsymbol{m}$ and R_B by:

$$1 - \exp(-\alpha \boldsymbol{M} d) = [1 - \exp(-\alpha \boldsymbol{m}\, d)]\,[1 + R_B \exp(-\alpha \boldsymbol{m}\, d)] \tag{A1}$$

Lechner *et al.*[24] analyze the measured QE of devices with low and high haze, in a manner very similar to that presented here. They incorporate all the enhancement of the *i*-layer absorption into the single parameter $\boldsymbol{M}$. They also determine the wavelength dependence of the enhancement factor, as we did, and discuss how it relates to the number of passes N, and quantitatively assess the optical losses as we do here. From Equation (A1), their $\boldsymbol{M}$ can be compared numerically with our $\boldsymbol{m}$ as follows: at 700 nm, where $\alpha = 2{\cdot}4 \times 10^{-3}\,\mathrm{cm}^{-1}$, for $d = 2{\cdot}8 \times 10^{-5}$ cm, $R_B = 0{\cdot}87$, and $\boldsymbol{m} = 3$, the corresponding enhancement factor is $\boldsymbol{M} = 5{\cdot}6$. If $R_B = 1$, then $\boldsymbol{M} = 6{\cdot}0 = 2\boldsymbol{m}$ since $[1 - \exp(-\alpha \boldsymbol{m}\, d)]\,[1 + \exp(-\alpha \boldsymbol{m}\, d)] = [1 - \exp(-2\alpha \boldsymbol{m}\, d)]$, which would indicate a doubling of the oblique light pass. Lechner *et al.*[24] relate the number of passes N to the enhancement $\boldsymbol{M}$ via the cosine of the average scattering angle $\theta = 55^\circ$, representing the average between the angle for critical scattering ($\sim 33^\circ$) and the maximum of 90°, or:

$$N = \boldsymbol{M} \cos\theta \tag{A2}$$

For the above example with $\boldsymbol{m} = 3$ and $\boldsymbol{M} = 5{\cdot}6$, this leads to $N = 3{\cdot}2$, or slightly more than 3 passes through the *i*-layer. Note that while in this example our $\boldsymbol{m}$ and the N of Lechner *et al.*[24] were nearly identical, this will not always be the case.

REFERENCES

1. Deckman H, Wronski C, Witske H, Yablonovitch E. Optically enhanced amorphous silicon solar cells. *Applied Physics Letters* 1983; **42**: 968–969.
2. Fujimoto K, Kawai H, Okamoto H, Hamakawa Y. Improvement in the efficiency of amorphous silicon solar cells utilizing the optical confinement effect by means of a TiO_2/Ag/SUS back-surface reflector. *Solar Cells* 1984; **11**: 357–366.
3. Banarjee A, Hoffman K, Xu X, Yang J, Guha S. Back reflector texture and stability issues in high efficiency multi-junction amorphous silicon alloy solar cells. *Proceedings of the 1st World Conference on Photovoltaic Energy Conversion*, IEEE, 1994; 539–543.
4. Tao G, Girwar B, Landweer G, Zeman M, Metselaar J. Enhanced light absorption in a-Si:H layers of solar cells by applying TCO/metal back contacts. *Materials Research Society Symposium Proceedings* 1993; **297**: 845–849.
5. Terzini E, Rubino A, de Rosa R, Addonizio M. The effect of ZnO sputtering deposition parameters on the performances of back reflector enhanced amorphous silicon solar cells. *Materials Research Society Symposium Proceedings* 1995; **377**: 681–686.
6. Hegedus S, Deng X. Analysis of optical enhancement in a-Si n-i-p solar cells using a detachable back reflector. *Proceedings of the 25th IEEE Photovoltaic Specialists Conference* 1996; 1061–1065.

7. Rech B *et al.* Texture etched ZnO:Al films as front contact and back reflector in amorphous silicon p-i-n and n-i-p solar cells. *Proceedings of the 26th IEEE Photovoltaic Specialists Conference* 1997; 619.
8. Ikeo I, Morooka H, Shinohara H, Takenouchi A, Takagi N, Arai Y. Fabrication and properties of flexible a-Si:H solar cells with textured Al-Si alloy electrodes. *Journal of Noncrystalline Solids* 1996; **198–200**: 1109–1112.
9. Schade H, Smith Z. Optical properties and quantum efficiency of *a*-$Si_{1-x}C_x$:H/a-Si:H solar cells. *Journal of Applied Physics* 1985; **57**: 568–574.
10. Wiedeman S, Morris J, Yang L. Optical losses in multi-junction *a*-Si:H based solar cells and modules. *Proceedings of the 21st IEEE Photovoltaic Specialists Conference* 1990; 1529–1534.
11. Hoffman K, Glatfelter T. An optical study of each layer in a-Si:H solar cells. *Proceedings of the 23rd IEEE Photovoltaic Specialists Conference* 1993; 986–999.
12. Leblanc F, Perrin J, Schmitt J. Numerical modeling of the optical properties of hydrogenated amorphous-silicon-based *p-i-n* solar cells deposited on rough transparent conducting oxide substrates. *Journal of Applied Physics* 1994; **75**: 1074–1087.
13. Sopori B, Madjdpour J, von Roedern B, Chen W, Hegedus S. Optical losses in amorphous silicon solar cells due to back reflectors. *Materials Research Society Symposium Proceedings* 1997; **467**: 777–782.
14. Schropp REI, Zeman M. Amorphous and Microcrystalline Silicon Solar Cells: Modeling, Materials and Device Technology. *Amorphous and Microcrystalline Silicon Solar Cells: Modeling, Materials and Device Technology*, Kluwer, Norwell, MA, USA, 1998; Chap. 7.
15. Hegedus S, Buchanan W, Liu X, Gordon R. Effect of textured tin oxide and zinc oxide substrates on the current generation in amorphous silicon solar cells. *Proceedings of the 25th IEEE Photovoltaic Specialists Conference* 1996; 1129–1132.
16. Hegedus S, Buchanan W, Eser E. Improving performance of superstrate p-i-n a-Si solar cells by optimization of n/TCO/metal back contacts. *Proceedings of the 26th IEEE Photovoltaic Specialists Conference* 1997; 603–606.
17. Garcia-Castaneda M, Sanchez-Machet H. An iterative and consistent method for the complex refraction index calculation of absorbent thin films. *Thin Solid Films* 1989; **176**: 69–72.
18. Hishikawa Y, Nakamura N, Tsuda S, Nakano S, Kishi Y, Kuwano Y. Interference-free determination of the optical absorption coefficient and the optical gap of amorphous silicon thin films. *Japan Journal of Applied Physics* 1991; **30**: 1008–1014.
19. Steibig H, Kreisel A, Winz K, Shultz N, Beneking C, Eickhoff Th, Wagner H. Spectral response modelling of a-Si:H solar cells using accurate light absorption profiles. *Proceedings of the 1st World Conference on Photovoltaic Energy Conversion*, IEEE, 1994; 603–606.
20. Morris J, Arya R, O'Dowd J, Wiedeman S. Absorption enhancement in hydrogenated amorphous silicon-based solar cells. *Journal of Applied Physics* 1990; **67**: 1079–1087.
21. Tao G, Girwar B, Landweer G, Zeman M, Metselaar J. Highly reflective TCO/back contact for a-Si:H solar cells. *Proceedings of the 11th European Photovoltaic Solar Energy Conference* 1992; 605–608.
22. Walker G, Hollingsworth R, Madan A. Determination of the efficiency enhancement due to scattering from rough TCO contact for a-Si:H p-i-n solar cells. *Materials Research Society Symposium Proceedings* 1987; **95**: 527–532.
23. Hishikawa Y, Maruyama E, Yata S, Tanaka M, Kiyama S, Tsuda S. Optical confinement in high-efficiency a-Si solar cells with textured surfaces. *Solar Energy Materials and Solar Cells* 1997; **49**: 143–148.
24. Lechner P, Geyer R, Schade H, Rech B, Muller J. Detailed accounting for quantum efficiency and optical losses in a-Si:H based solar cells. *Proceedings of the 28th IEEE Photovoltaic Specialists Conference* 2000; 861–864.

